THE SURVEY FOR IONIZATION IN NEUTRAL-GAS GALAXIES:
III. DIFFUSE, WARM IONIZED MEDIUM AND ESCAPE OF IONIZING RADIATION

M. S. Oey[1], G. R. Meurer[2], S. Yelda[1,3], E. J. Furst[4], S. M. Caballero-Nieves[1,5], D. J. Hanish[2], E. M. Levesque[6], D. A. Thilker[2], G. L. Walth[7], J. Bland-Hawthorn[8] M. A. Dopita[9], H. C. Ferguson[11], T. M. Heckman[2], M. T. Doyle[10], M. J. Drinkwater[10], K. C. Freeman[9], R. C. Kennicutt, Jr.[12], V. A. Kilborn[13,15], P. M. Knezek[14], B. Koribalski[15], M. Meyer[11], M. E. Putman[1], E. V. Ryan-Weber[12], R. C. Smith[17], L. Staveley-Smith[15], R. L. Webster[18], J. Werk[1], M. A. Zwaan[16],

Accepted 28-February-2007 to the Astrophysical Journal

ABSTRACT

We use the first data release from the SINGG Hα survey of H I-selected galaxies to study the quantitative behavior of the diffuse, warm ionized medium (WIM) across the range of properties represented by these 109 galaxies. The mean fraction $f_{\rm WIM}$ of diffuse ionized gas in this sample is 0.59 ± 0.19, slightly higher than found in previous samples. Since lower surface-brightness galaxies tend to have higher $f_{\rm WIM}$, we believe that most of this difference is due to selection effects favoring large, optically-bright, nearby galaxies with high star-formation rates. As found in previous studies, there is no appreciable correlation with Hubble type or total star-formation rate. However, we find that starburst galaxies, defined here by an Hα surface brightness $> 2.5 \times 10^{39}$ erg s^{-1} kpc^{-2} within the Hα half-light radius, do show much lower fractions of diffuse Hα emission. The cause apparently is not dominated by a lower fraction of field OB stars. However, it is qualitatively consistent with an expected escape of ionizing radiation above a threshold star-formation rate, predicted from our model in which the ISM is shredded by pressure-driven supernova feedback. The H I gas fractions in the starburst galaxies are also lower, suggesting that the starbursts are consuming and ionizing all the gas, and thus promoting regions of density-bounded ionization. If true, these effects imply that some amount of Lyman continuum radiation is escaping from most starburst galaxies, and that WIM properties and outflows from mechanical feedback are likely to be pressure-driven. However, in view of previous studies showing that the escape fraction of ionizing radiation is generally low, it is likely that other factors also drive the low fractions of diffuse ionized gas in starbursts.

Subject headings: ISM: evolution — H II regions — galaxies: evolution — intergalactic medium — galaxies: ISM — galaxies: starburst

1. INTRODUCTION

Ionizing radiation is one of the three major feedback processes from massive stars, alongside mechanical and nucleosynthetic effects, that are propagated by the most massive stellar populations. The hot temperatures and powerful luminosities of these stars yield prodigious emission rates of H-ionizing photons ($48 \lesssim \log Q_0/{\rm s}^{-1} \lesssim 50$), thereby producing luminous regions of ionized gas that are visible at great distances.

Because of the high ionizing luminosities, ranging up to $\sim 3 \times 10^{38}$ erg s^{-1} for individual stars, radiative feedback is energetically important and has fundamental con-

[1] University of Michigan, Department of Astronomy, 830 Dennison Building, Ann Arbor, MI 48109-1042

[2] Johns Hopkins University, Department of Physics and Astronomy, 3400 N. Charles St., Baltimore, MD 21218-2686

[3] Present address: University of California, Department of Physics and Astronomy, P. O. Box 951547, Los Angeles, CA 90095-1547

[4] Participant in the Research Experience for Undergraduates program, Northern Arizona University; Bucknell University, Department of Physics, Lewisburg, PA 17837; Present address: 344 Greenlow Rd., Catonsville, MD 21228

[5] Present address: Georgia State University, Department of Physics and Astronomy, P. O. Box 4106, Atlanta, GA 30303

[6] Massachusetts Institute of Technology, Department of Physics, 77 Massachusetts Ave., Cambridge, MA 02139; Present address: Institute for Astronomy, 2680 Woodlawn Dr., Honolulu, HI 96822

[7] Observatories of the Carnegie Institution of Washington, 813 Santa Barbara St., Pasadena, CA 91101

[8] Anglo-Australian Observatory, P. O. Box 296, Epping, NSW 2121, Australia

[9] Australian National University, Research School of Astronomy and Astrophysics, Cotter Road, Weston Creek, ACT 2611, Australia

[10] University of Queensland, Department of Physics, St. Lucia, QLD 4072, Australia

[11] Space Telescope Science Institute, 3700 San Martin Dr., Baltimore, MD 21218

[12] Institute of Astronomy, University of Cambridge, Madingley Road, Cambridge, CB3 0HA, United Kingdom

[13] Swinburne University of Technology, Centre for Astrophysics and Supercomputing, Mail 39, P. O. Box 218, Hawthorn, VIC 3122, Australia

[14] WIYN, Inc., 950 N. Cherry Ave., Tucson, AZ 85721

[15] Australia Telescope National Facility, CSIRO, P. O. Box 76, Epping, NSW 1710, Australia

[16] European Southern Observatory, Karl-Schwarzschild-Str. 2, D-85748 Garching b. München, Germany

[17] Cerro Tololo Inter-American Observatory, Casilla 603, La Serena, Chile

[18] University of Melbourne, School of Physics, Parkville, VIC 3010, Australia

sequences for the evolution of the interstellar medium (ISM) of host galaxies and the surrounding intergalactic medium (IGM). The warm (10^4 K) component of the multiphase ISM, which is the most massive component of ionized gas in galaxies (Walterbos 1998), is thought to result primarily from radiative feedback, and the resulting ISM phase balance strongly affects evolutionary processes like star formation and ISM gas dynamics. Furthermore, of intense current interest, the escape fraction and energies of ionizing photons from galaxies are crucial to the ionization state of the IGM and reionization of the early universe. With current rapid advances in absorption-line and emission-line probes of the high-redshift Universe, we are urgently in need of a quantitative understanding of radiative feedback processes to interpret cosmic history and galaxy formation.

The total Hα emission from star-forming galaxies is divided roughly in half, between classical, discrete H II regions, and the diffuse, warm ionized medium (WIM), often also referred to as diffuse ionized gas (DIG). The WIM is generally thought to be ionized by massive stars, too, since they are the only candidate capable of providing the necessary power (Reynolds 1984). However, the ionization and energetics of the WIM are poorly understood. For example, does the WIM always comprise around 40% of the total Hα emission in star-forming galaxies, as suggested by the extant observations (e.g., Wang et al. 1999; Hoopes et al. 1996; Ferguson et al. 1996)? If so, why would the WIM fraction be independent of galaxy parameters like star formation rate and Hubble type? It is thought that roughly half of the diffuse ionization originates from Lyman continuum radiation escaping from ordinary H II regions (e.g., Oey & Kennicutt 1997), and half from massive stars in the field (e.g., Oey et al. 2004; Hoopes & Walterbos 2000). While there is a spatial correlation between H II regions and diffuse emission (e.g., Zurita et al. 2002; Ferguson et al. 1996; Hoopes et al. 1996), Dopita et al. (2006) also suggest that about half of the WIM simply may consist of extremely evolved, filamentary H II regions that may be difficult to detect as such, and therefore are assigned to the WIM. It also appears that photoionization by OB stars cannot exclusively explain the ionization state of the WIM (e.g., Collins & Rand 2001; Reynolds et al. 1999). Thus, a clearer understanding of the ionization processes and radiative transfer is needed to understand the true role of massive stars. And, if ionizing radiation escapes from H II regions to ionize the WIM, then does it also escape from galaxies altogether, thereby affecting the ionization state of the IGM, as predicted by, e.g., Clarke & Oey (2002)? If this occurs, then how commonplace is it, and under what conditions does it happen?

The first, necessary step is to empirically quantify the WIM properties across all classes of star-forming galaxies, which is now possible with a new, definitive dataset: the Survey for Ionization in Neutral-Gas Galaxies (SINGG; Meurer et al. 2006; hereafter Paper I). SINGG is an Hα and R-band imaging survey of 468 galaxies selected only on the basis of their H I emission from the H I Parkes All-Sky Survey (HiPASS; Barnes 2001). Since HiPASS is a blind H I survey of the entire southern sky within radial velocity 12,700 km s^{-1}, the detected galaxies span essen-

tially the entire range of star formation properties that occur, given an adequate gas supply. SINGG consists of a subsample of the HiPASS galaxies, up to radial velocities of 10,000 km s^{-1}, and uniformly sampling the H I mass range $7.0 < \log(M_{\mathrm{HI}}/\mathrm{M}_\odot) < 11.0$. It is therefore possible to investigate the global radiative feedback effects essentially *across a complete parameter space of gas-rich galaxy properties.*

With the SINGG dataset, we can quantify parameters like the fraction of total Hα luminosity occupied by the WIM, and its relation to galaxy properties like star-formation rate, H I mass, and stellar luminosity. The patterns that emerge from the data will clarify the physical processes associated with this major component of the ISM.

2. Hα DATA ANALYSIS

We adopt the common definition of the WIM, namely, that it is the diffuse Hα emission in excess, and outside of, the classical H II regions (e.g., Hoopes et al. 1996). Since there are many ways of defining H II region boundaries, any quantitative results on the WIM parameters will necessarily depend on the methods used, and so quantitative results from any study of the WIM should be treated with appropriate caution. Nevertheless, as we demonstrate below, our general qualitative results are robust. Future studies incorporating an additional parameter to define the WIM, such as kinematic line widths, may yield more robust and useful definitions of the WIM (Shopbell & Bland-Hawthorn 1998).

We report here on results from 109 galaxies in the SINGG Release 1 (SR1) subset (Paper I). These generally correspond to a range in H I mass of $7.5 < \log(M_{\mathrm{HI}}/\mathrm{M}_\odot) < 10.6$, although some targets turned out to have multiple galaxies in the field of a single H I detection, and so for these siblings we have only an upper limit on M_{HI}. The galaxies have distances of 4 – 73 Mpc, with most in the range 10 – 20 Mpc (see Paper I; Hanish et al. 2006). Preliminary data reduction and flux calibration for the sample were carried out by the SINGG pipeline (see Paper I), including Galactic and internal extinction corrections, and corrections for [N II] inclusion in the Hα filter bandpasses.

An important parameter for this sample of Hα observations is the star formation per unit area, or star-formation intensity (SFI[*]). For much of the work that follows, we adopt three bins of SFI, corresponding to the effective Hα surface brightness $\Sigma_{\mathrm{H}\alpha}$ within the star-forming disks, which is given by:

$$\Sigma_{\mathrm{H}\alpha} = \frac{L_{\mathrm{H}\alpha}}{2\pi R_{e,\mathrm{H}\alpha}^2} \quad , \qquad (1)$$

where $R_{e,\mathrm{H}\alpha}$ is the effective (half-light) radius in Hα from Paper I. We refer to galaxies having $38.4 < \log\Sigma_{\mathrm{H}\alpha} \le 39.4$ as "normal," those having $\log\Sigma_{\mathrm{H}\alpha} > 39.4$ as "starburst," and those having $\log\Sigma_{\mathrm{H}\alpha} \le 38.4$ as "sparse." This binning, in units of $\log\mathrm{erg\,s^{-1}\,kpc^{-2}}$, was chosen to assign galaxies whose star-forming disks are mostly packed with merging H II regions as "starbursts." This is much more generous than Heckman's (2005) definition in terms of SFI; using the conversion from Kennicutt et al. (1994) to relate

---

[*]Paper I abbreviated the star-formation per unit area as 'SFA.'

SFR and Hα luminosity:

$$\text{SFR } (\text{M}_\odot \text{ yr}^{-1}) = L_{\text{H}\alpha} \text{ (erg s}^{-1}) \text{ / } 1.26 \times 10^{41} \quad , \quad (2)$$

our criterion of $\Sigma_{\text{H}\alpha} > 2.5 \times 10^{39}$ erg s^{-1} kpc^{-2} corresponds to 0.02 M$_\odot$ yr^{-1} kpc^{-2}, whereas Heckman gives a range of $1 - 100$ M$_\odot$ yr^{-1} kpc^{-2} for typical starbursts. However, that definition is largely based on small portions of galaxies containg a starburst (Meurer et al. 1997). Other common starburst definitions include EW$_{50}$(Hα) $>$ 50 Å, as in Paper I, which refers to the equivalent width within the Hα half-light radius. Our adopted starburst definition based on $\Sigma_{\text{H}\alpha}$ is more appropriate to the global properties used here: Meurer (2007, in preparation) shows that a single threshold of $\Sigma_{\text{H}\alpha} \gtrsim 39.4$ is sufficient to isolate the well-known starbursts in the SR1 sample, and is "cleaner" than an equivalent EW$_{50}$(Hα) cut. We therefore feel that an Hα surface brightness, or intensity criterion suggested by Heckman (2005) is intuitively the most appropriate, but readers should consider differences in definitions when considering the literature on starbursts. We also define a category of "nuclear starbursts," which are galaxies whose star formation is strongly dominated by the nuclear region; these are visually assigned. Figure 1 shows example Hα images of each star formation category.

Similar to the analysis by Wang et al. (1999), Figure 2a shows the Hα surface brightness distributions in Hα flux per pixel $S_{\text{H}\alpha}$, after smoothing the Hα images with a 9×9 pixel (3.87$''$ diameter) box car. We include only pixels showing emission above a detection limit of 2σ above the background level in each image, which was derived as discussed in Paper I. The galaxies are color-coded according to $\Sigma_{\text{H}\alpha}$, with starbursts at the red extreme, and the lowest $\Sigma_{\text{H}\alpha}$ at the violet and black extreme. It is apparent that the starbursts show significantly flatter slopes at lower $S_{\text{H}\alpha}$, indicating that they have smaller relative contributions of diffuse Hα emission compared to the H II regions. We determined the slopes α using a least-squares fit to the logarithmic quantities plotted in Figure 2b, within the range $-1.5 < \log(S_{\text{H}\alpha}/S_{\text{H}\alpha,\text{eff}}) < 0.0$. The normalizing surface brightness $S_{\text{H}\alpha,\text{eff}}$ corresponds to the isophote that includes half the total Hα flux of each object. Figure 2b shows these fitted slopes as a function of $S_{\text{H}\alpha}$, color-coded as before, again demonstrating the trend of flattening slope with increasing SFI for the whole sample.

We can examine the conventional fraction f_{WIM} of diffuse Hα emission by defining the spatial division between the WIM and H II regions, as is commonly done. Because the diffuse Hα emission of the WIM is the emission in excess, and outside of, the classical H II regions, defining the WIM therefore requires defining the H II regions as well. Since photometry of irregular, extended H II regions is tricky, we compared some of the different algorithms available for automated H II region identification and photometry (e.g., McCall et al. 1996; Knapen 1998; Thilker et al. 2000). The HIIphot software by Thilker et al. (2000) yields reliable nebular catalogs, and we opted to use this code, based on the H II region definition criteria and user control over vital parameters. HIIphot then identifies objects above a threshold signal-to-noise, and determines the boundaries according to a user-defined, limiting radial gradient in Hα surface brightness, known as the "terminal gradient". H II

region luminosities are computed within the boundaries, subtracting the local background, and the remaining diffuse Hα background and exterior emission is defined to be the WIM. The background emission for the nebular regions is computed from a two-dimensional interpolation scheme described by Thilker et al. (2000). We modified the original version of the code to calculate the total WIM luminosity and fraction of the Hα luminosity. The HIIphot algorithms are more fully described by Thilker et al. (2000), and we also discuss them further below.

We first created blanking masks to exclude foreground stars and other spurious features from the analysis. The total galaxy apertures were the same elliptical apertures defined by Paper I, based on the galaxy R-band isophotes. In a few cases where the galaxy's angular size exceeded that required by the standard aperture-defining algorithm, we redefined the apertures by hand, using the HIIphot interface for that purpose. Our independent measurements agree well; the mean ratio of galaxy Hα luminosities measured by Paper I, to those measured in this work, is $L_{\text{H}\alpha}(\text{Paper I})/\text{L}_{\text{H}\alpha}(\text{HIIphot}) = 1.07 \pm 0.29$.

The HIIphot terminal gradient criterion for defining the H II region boundaries depends on seeing conditions and distance, because classical H II regions have a strong drop in surface brightness at the Strömgren edge. Thus, for high spatial resolution in nearby galaxies and/or good seeing, the terminal gradient that defines the object edge has a higher value than for low resolution. We therefore allocated the terminal gradients for each galaxy based on visual inspection, with values ranging over $0.5 - 9.0$ pc cm^{-6} pc^{-1}. We find that the resulting diffuse Hα fractions f_{WIM} are not highly sensitive to the adopted terminal gradient; f_{WIM} typically varies by $\lesssim 0.1$ for termgrad variations of 25–50%. Within a distance of ~ 20 Mpc, we see the full range of terminal gradients (Figure 3). Beyond that distance, however, the terminal gradients converge to about 1 pc cm^{-6} pc^{-1}, again because the spatial resolution limits the H II region boundary definitions and resulting photometry. As has been noted in the past (e.g., Deharveng et al. 1988), the spatial resolution affects H II region luminosity functions for distant galaxies. However, the total photometry of the H II regions and WIM apparently are not strongly affected, since HIIphot computes a diffuse background for the objects, and also because the WIM has a larger scale height than the H II regions, which lessens the importance of line-of-sight confusion between H II regions and WIM. Figure 4 shows the WIM fraction as a function of distance, and there is no apparent correlation, demonstrating that effects due to spatial resolution are minimal. We therefore include the entire SR1 sample over the full distance range in our study of the WIM behavior.

Figure 4 shows that the starburst galaxies have lower WIM fractions than the rest of the sample. Since the WIM is usually defined simply as the remainder of a galaxy's Hα emission outside of the discrete H II regions, the best way to measure its luminosity is by careful photometry and subtraction of the H II region luminosities (e.g., Hoopes et al. 1996). We believe that HIIphot is currently the best automated routine for nebular photometry because it carries out a detailed definition of the H II region boundaries, and it also accounts for varying background emission levels (see above). The latter are a problem for some methods,
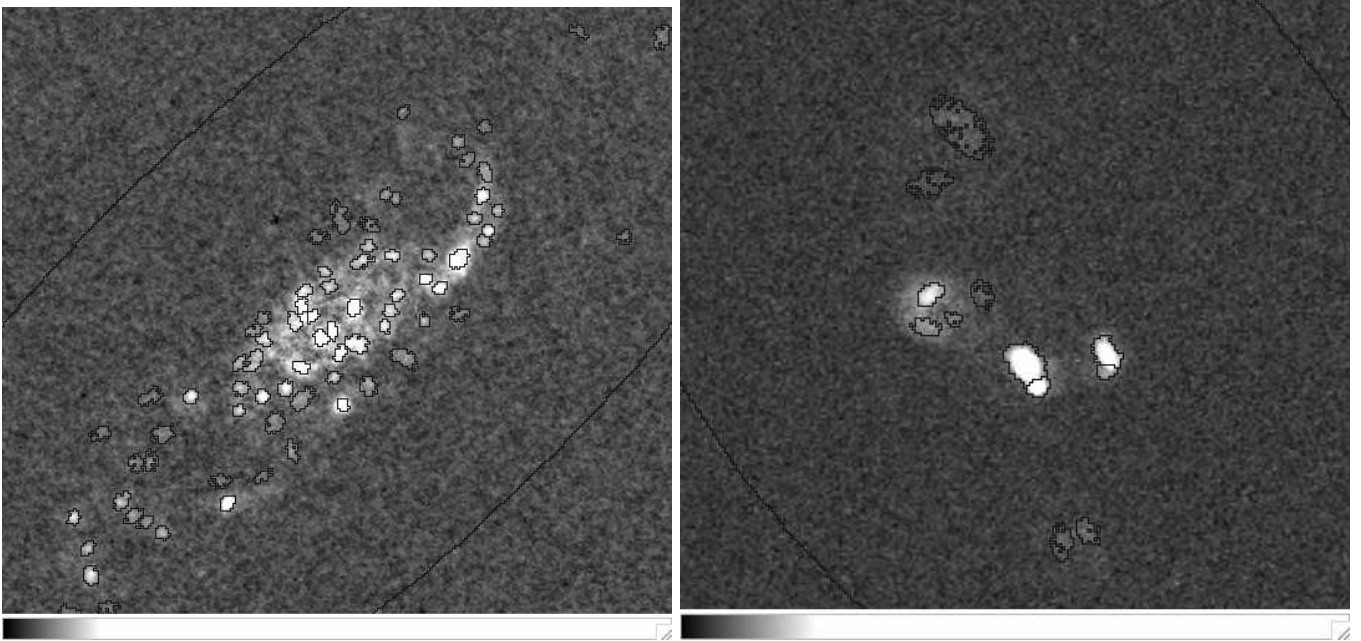
FIG. 1.— Representative examples of the galaxy categories. (a) "Normal:" J0412+02, $\log\Sigma_{H\alpha} = 38.92$; (b) "Sparse:" J0031–22, $\log\Sigma_{H\alpha} = 38.26$; (c) "Starburst:" J0355–42, $\log\Sigma_{H\alpha} = 39.40$; (d) "Nuclear Starburst:" J0209–10:S2. $\Sigma_{H\alpha}$ is quoted in units of erg s^{-1} kpc^{-2}. HII region boundaries defined by HIIphot are outlined in black. The large elliptical apertures indicated by the black lines around the galaxies are those defined from R-band images by Paper I (their r_{max}) for the total galaxy flux measurements. The images are roughly 1.8$'$ square, with north up and east to the left; all are displayed with the same gray scale.
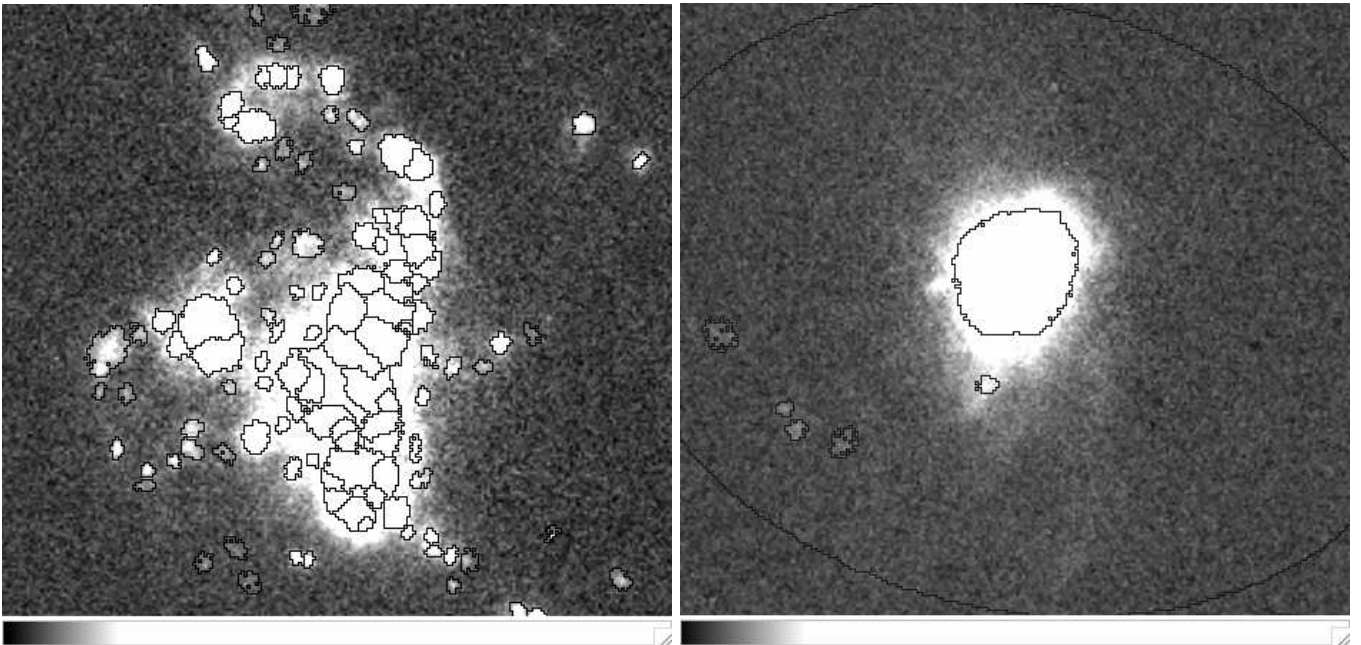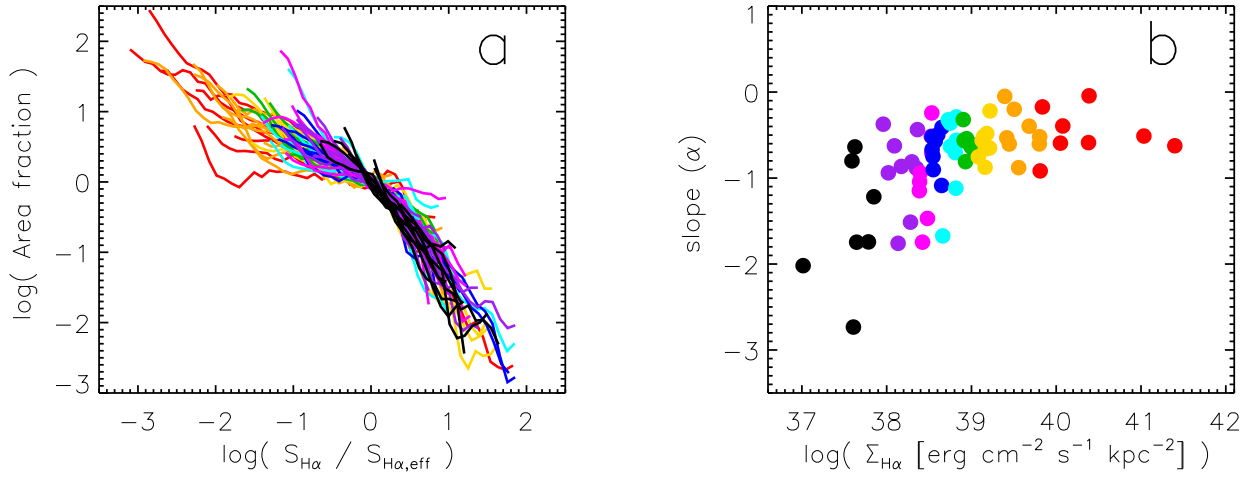

FIG. 1.— continued

Fig. 2.— Differential Hα surface brightness distributions for the individual galaxies (Figure 2a), color-coded according to $\Sigma_{H\alpha}$; starburst galaxies are plotted in red, and galaxies with the lowest $S_{H\alpha}$ in violet and black. The distributions are shown as fractional area of all pixels above the detection threshold, and $S_{H\alpha}$ is normalized to $S_{H\alpha,eff}$, the value above which the distribution accounts for half the Hα flux. The surface brightness distributions are also normalized at this value. Figure 2b shows the slopes of the low-luminosity end of the Hα surface brightness distributions as a function of mean total $\Sigma_{H\alpha}$.
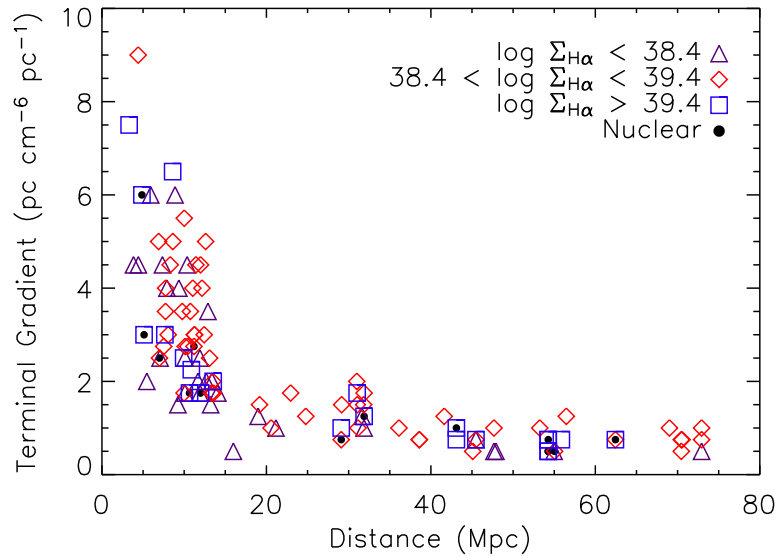

Fig. 3.— Adopted HIIphot terminal gradients vs distance. The symbols show star-formation intensity, as measured by the Hα surface brightness $\Sigma_{H\alpha}$, as shown. Galaxies dominated by nuclear star formation are indicated by the central black dots.
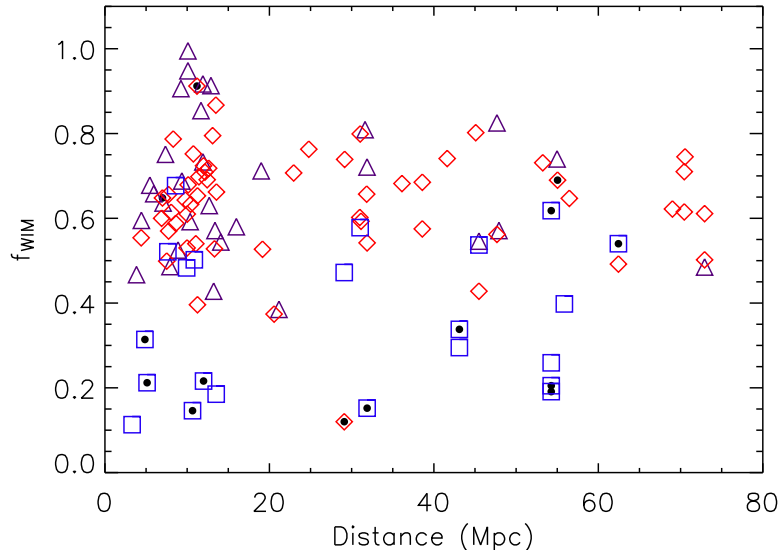
Fig. 4.— Hα fraction of diffuse, warm ionized medium vs galaxy distance. Symbols are as in Figure 3.

like those that isolate the WIM by assigning it a fixed surface brightness level; Thilker et al. (2002) provide detailed discussion of various methods that have been used for defining diffuse Hα emission.

Figure 5 shows WIM fraction vs galaxy angle of inclination i, with symbols as in Figure 3. There are no correlations, with all star-formation categories occurring at all angles of inclination. The measured $f_{\rm WIM}$ also shows no selection bias based on i. Although photometry of the H II regions, which are limited to the disk plane, becomes problematic at large i as the objects merge in the line of sight, photometry of the WIM appears to be not strongly affected. The HIIphot algorithm, in particular, minimizes inclination effects because it interpolates local background values for H II regions. As described above, these background values are included in the WIM photometry. Our results are consistent with those of Thilker et al. (2002), who also found no apparent biases resulting from galaxy inclination. Furthermore, the WIM often has a large scale height relative to the classical H II regions (e.g., Rossa & Dettmar 2003; Collins & Rand 2001; Veilleux et al. 1995), which will tend to counteract inclination effects.

Since the crowding of H II regions at high inclinations mimics the crowding seen in starburst galaxies, the normal $f_{\rm WIM}$ values measured for the edge-on galaxies, in contrast to the starbursts, is also strong evidence of a real reduction in $f_{\rm WIM}$ for the starbursts. In addition, note that the contaminating [N II] emission is on the order of 3 times higher in the WIM than in the H II regions (e.g., Hoopes & Walterbos 2003; Collins & Rand 2001; Shopbell & Bland-Hawthorn 1998). Thus, the true ratio of Hα emission $L_{\rm Hα}({\rm WIM})/L_{\rm Hα}({\rm HII})$ is less than the apparent relative fluxes observed in the Hα filters. Furthermore, Figures 6a and b compare, respectively, the HIIphot boundaries for the same starburst galaxy for the standard run, and a run for which the output has been forced to match a value of

$f_{\rm WIM}$ typical of the entire sample. For the latter, we obtain $f_{\rm WIM}= 0.54$ with an adopted terminal gradient that is over 50 times its value for the standard run. Figure 6c shows another standard run for a normal galaxy having a similar distance. It is apparent that a gross difference in nebular boundary criteria is necessary to force the starbursts to match the normal galaxies in $f_{\rm WIM}$. Thus, our result of a lower fraction of WIM emission from starbursts appears to be robust, although we do caution that specific, quantitative measurements of $f_{\rm WIM}$ are dependent on the method used to define and distinguish diffuse Hα emission from H II regions; readers should bear this in mind when comparing results between different studies.

3. RELATION OF WIM TO GALAXY PROPERTIES

Table 1 lists the SINGG SR1 sample of galaxies.[†] For convenience, we repeat several fundamental parameters from Paper I here. As detailed in Paper I, H I-related quantities were derived from HIPASS data, in particular, HICAT, the full HIPASS catalog (Meyer, et al. 2004), and the HIPASS Bright Galaxy Catalog (Koribalski et al. 2004). Distances were derived primarily from the H I radial velocities using the distance model of Mould et al. (2000), with optical distances to the nearest sources taken from the Catalog of Neighboring Galaxies (Karachentsev et al. 2004). Readers are referred to Paper I for further details regarding SINGG catalogued quantities. The columns in Table 1 are as follows: (1) HIPASS designation, (2) optical identification, (3) Hubble type, (4) distance, (5) inclination angle i, (6) HIIphot terminal gradient, (7) H I mass $M_{\rm HI}$, (8) R-band luminosity L_R, (9) Hα luminosity $L_{\rm Hα}$, (10) Hα surface brightness $\Sigma_{\rm Hα}$, (11) Hα diffuse fraction $f_{\rm WIM}$, and (12) critical star-formation rate (see below). All quantities are in the SINGG database and presented by Paper I and Hanish et al. (2006), except for columns 6, and 9 – 14, which are derived in this work. Our

[†]We omit the multiple source J0514–61 owing to processing problems, and so our sample has only 109 galaxies instead of the full SR1 sample.
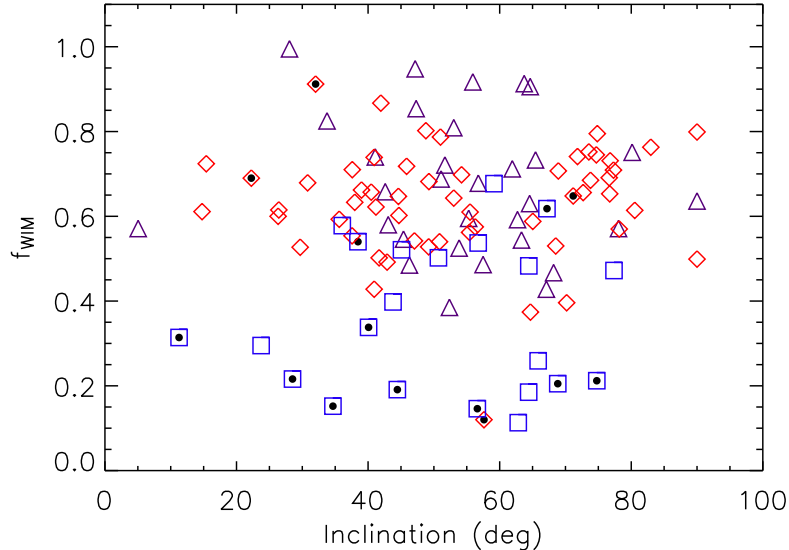
FIG. 5.— WIM fraction vs galaxy angle of inclination. Symbols for different star-formation categories are as in Figure 3.

Hα luminosities are corrected for Galactic and internal extinction using the same values as those in Paper I.

We generally confirm earlier findings that the fraction of Hα luminosity due to the WIM is largely independent of galaxy type, with the exception of the starburst galaxies, as described above. There is also a general trend of decreasing $f_{\rm WIM}$ with increasing R surface brightness (Figure 7). Helmboldt et al. (2005) and O'Neil et al. (2006) also report that low surface-brightness galaxies tend toward higher diffuse fractions. Here, we see a much larger scatter in $f_{\rm WIM}$ for low surface-brightness galaxies. This scatter may be due to uncertainties in continuum subtraction, which is more important in these galaxies. It is apparently not caused by variations in the HIIphot terminal gradient parameter, when comparing outliers with typical galaxies. For the 109 H I-selected galaxies in SINGG SR1, the mean diffuse fraction is 0.59±0.19. This value is somewhat higher than the typical ∼40% value found for other nearby galaxies (e.g., Thilker et al. 2002; Zurita et al. 2000; Ferguson et al. 1996). Since most of the previous studies favored nearby, high surface-brightness, actively star-forming galaxies, we believe that some of this difference is due to this optical selection effect. Furthermore, most of those nearby galaxies have large angular extents over several arcminutes, and the galaxy apertures used for the total Hα luminosity measurements were generally smaller in physical size than those in the SINGG survey (see Paper I). We note that Helmboldt et al. (2005) similarly studied an H I-selected sample and found typical $f_{\rm WIM} \sim 0.45$; however, their $f_{\rm WIM}$ were measured within the R-band half-light radii. Furthermore, the absolute measured value of $f_{\rm WIM}$ also likely depends on the depth of the Hα observations, since fainter diffuse emission may be detected with deeper imaging. The SINGG survey typically has sensitivity to an emission measure of 1.4 pc cm^{-6}, or 2.21×10^{-17} erg s^{-1} cm^{-2} arcsec^{-2} (Paper I), which is

deeper than many earlier studies, although stated depth limits depend on factors like background subtraction for any such work. All of the above effects are likely contributors to our higher mean $f_{\rm WIM}$ value for the SR1 sample, and further detailed investigation is necessary to evaluate these effects. There may also be some systematic measurement bias due to our specific definition and algorithm for identifying the WIM relative to other studies, as discussed above. However, we emphasize that this is the largest uniform study of the WIM to date, and it also benefits from the lack of any optical biases in sample selection.

Figure 8 shows $f_{\rm WIM}$ for the different Hubble types. Intermediate types are assigned to the earlier type, for example, Sbc galaxies are binned with Sb galaxies. Sm types are binned with Sd galaxies, and barred and non-barred types are binned together. The Hubble types are simply those from the NED[‡] database. In all of our analyses, including Figure 8, we see that the nuclear starbursts tend to be less confined to the parameter space occupied by the rest of the sample. Apparently, nuclear starbursts take place in many different galaxy conditions, and thus the star formation represented by such events is not closely related to non-nuclear star-formation properties, the latter of which are linked to the parent galaxies' global parameters.

Considering the remainder of the galaxies in Figure 8, there appears to be no correlation in the mean $f_{\rm WIM}$ with Hubble type, although the scatter in $f_{\rm WIM}$ tends to increase for late types. Table 2 gives the means and standard deviations for different galaxy classes, along with the number of galaxies N, averaged in each class. We again see that starbursts have systematically lower diffuse fractions across all galaxy types. We discuss this further below.

Figure 9 shows the Hα surface brightness vs Hubble type for the sample. Although late-type galaxies are often said to have the highest SFR per unit area, we see that the mean SFI is highest for Sb galaxies, again with the scat-
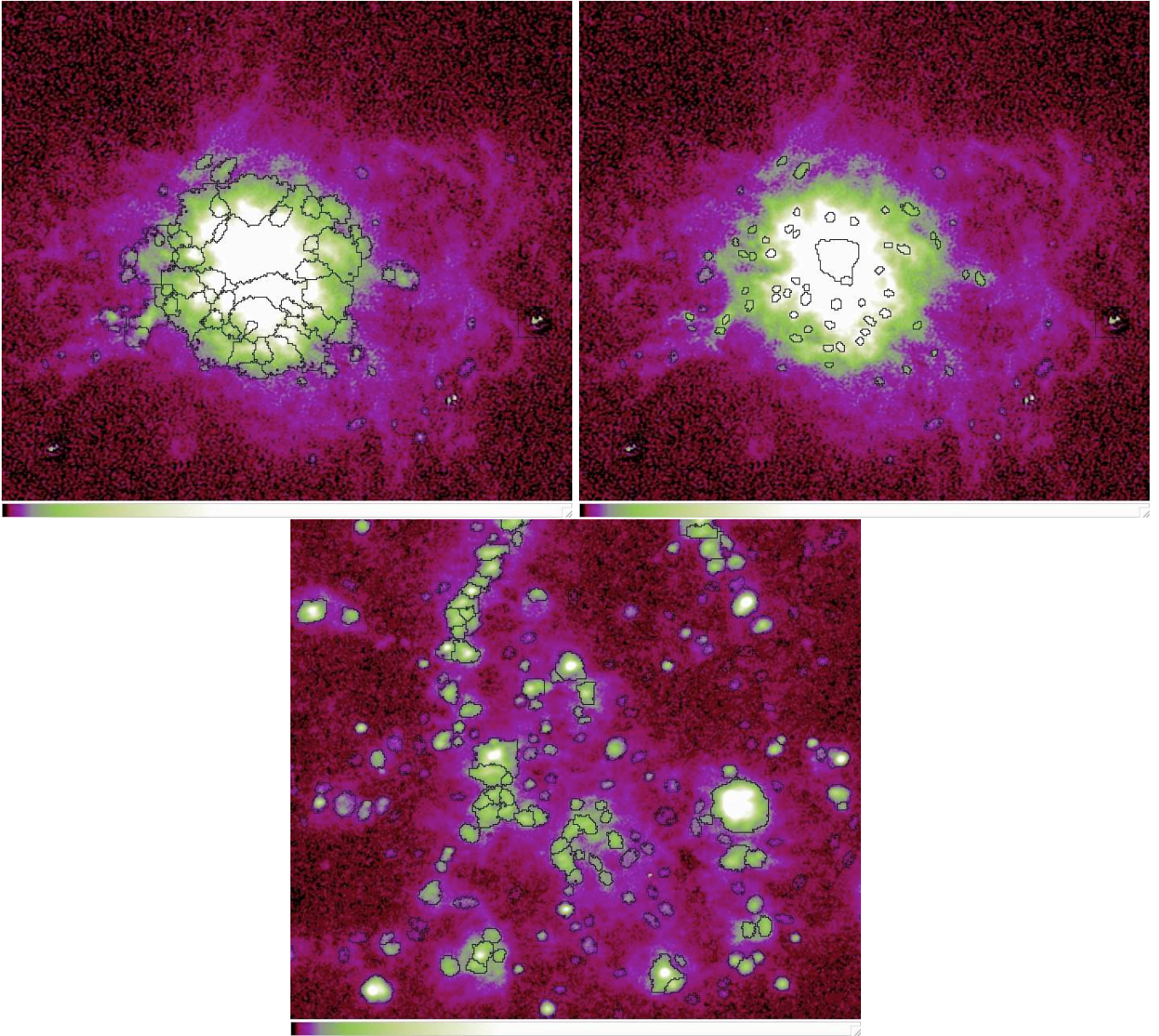
FIG. 6.— Figure 6a shows nebular boundaries for starburst galaxy J1339-31A for the standard run (termgrad = 7.5 pc cm^{-6} pc^{-1}, f_{WIM} = 0.11); Figure 6b shows J1339-31A for a run that forces f_{WIM} to a typical sample value (termgrad = 500 pc cm^{-6} pc^{-1}, f_{WIM} = 0.54); and Figure 6c shows the standard run for a normal galaxy having a similar distance, J1318-21 (termgrad = 5 pc cm^{-6} pc^{-1}, f_{WIM} = 0.60). All images are displayed with the same scales and color table. [This figure is displayed in color in the on-line edition.]

Fig. 7.— f_{WIM} as a function of R surface brightness. Symbols are as in Figure 3.

Fig. 8.— WIM fraction for galaxy Hubble types. Symbols for different star-formation categories are as in Figure 3.

TABLE 2
MEAN WIM FRACTIONS

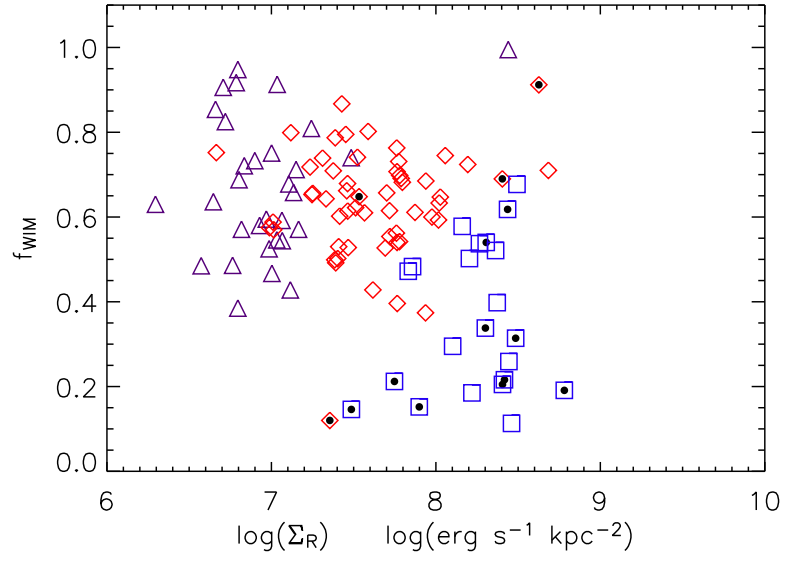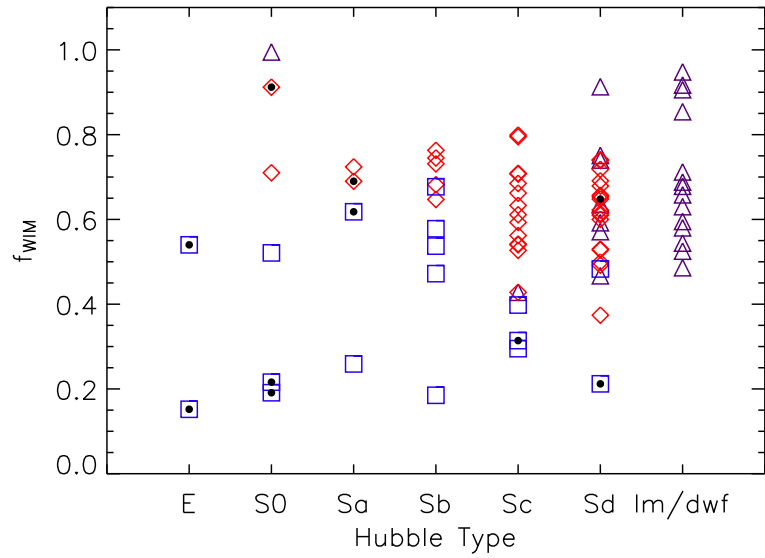| Category	$< f_{\mathrm{WIM}} >$	std dev	N
All SR1	0.59	0.19	109
E, S0, Sa[a]	0.54	0.29	12
Sb	0.60	0.17	10
Sc	0.57	0.15	18
Sd/Sm	0.61	0.14	26
Im/dwf	0.65	0.18	24
$\log \Sigma_{\mathrm{H}\alpha} \leq 38.4$[b]	0.67	0.16	31
$38.4 < \log \Sigma_{\mathrm{H}\alpha} \leq 39.4$[b]	0.63	0.13	56
$39.4 < \log \Sigma_{\mathrm{H}\alpha}$[b]	0.36	0.18	22
Nuclear	0.38	0.25	14

[a]Most of the E, S0, and Sa galaxies in this sample are dominated by nuclear star formation (see Figure 8).

[b]$\Sigma_{\mathrm{H}\alpha}$ in units of erg s^{-1} kpc^{-2}.

ter increasing with later Hubble type. Kennicutt (1998) notes that late-type galaxies tend to have more extended star-forming disks, and that characterizations across the Hubble sequence are dependent on how star formation is parameterized relative to the parent galaxy properties. He shows that it is the global Hα equivalent width that systematically increases toward later galaxy types, which is also seen in our data.

Since the WIM represents ionization of the neutral ISM, we might expect to find a relationship between the diffuse Hα fraction and galaxy H I content. Figure 10 shows f_{WIM} vs M_{HI}/L_R, the H I mass normalized by the R luminosity, which is a measure of galaxy H I gas fraction. Note that for 28 galaxies, there are only upper limits on M_{HI}, since these are multiple objects encompassed within the target HIPASS beams. A large scatter in f_{WIM} is evident in Figure 10. There is no apparent relation between f_{WIM} and neutral gas fraction, except for a few galaxies having the lowest values of M_{HI}/L_R, which also show the lowest diffuse fractions. Closer inspection shows that these are starburst galaxies, and again, that *ordinary starbursts as a group show both lower diffuse fractions and lower H I gas fractions.*

Figure 11 shows the Hα diffuse fraction vs star formation intensity, with symbols now corresponding to H I gas fraction, M_{HI}/L_R. We see an anti-correlation that is largely defined by the starbursts at $\log \Sigma_{\mathrm{H}\alpha} > 39.4$; the non-starburst galaxies show little, if any, trend in f_{WIM} with $\Sigma_{\mathrm{H}\alpha}$. Interestingly, Figure 11 shows that the galaxies with the *lowest* H I gas fractions define an upper edge in the f_{WIM} – SFI space, whereas galaxies with the largest M_{HI}/L_R have low star formation intensities and wide range of f_{WIM}. There is a continuous relation between H I gas fraction, star formation intensity, and f_{WIM} for the galaxies near this edge.

4. ESCAPE OF IONIZING RADIATION?

Why do the ordinary starbursts show both lower Hα diffuse fractions *and* lower H I gas fractions? Given the higher ionizing luminosities in starbursts, the lower H I fraction might not be surprising. However, we might then have

expected a *higher* f_{WIM} if the lower H I fraction were due to ionization by the starbursts. Since this is not observed, we must consider other possibilities: (1) An important ionization source of the WIM has been reduced, for example, (1a) less ionizing radiation escaping from strongly obscured starbursts; or (1b) less ionizing radiation available from a reduced population of field OB stars. Alternatively, (2) some fraction of ionizing radiation escapes from these galaxies, either (2a) under-ionizing the WIM, or (2b) fully ionizing it in a density-bounded situation.

While we have no data at present to evaluate possibility (1a) above, we can examine possibility (1b) by assuming simple global parameterizations for the behavior of massive stars in the field. Recent work suggests that field O and B stars ionize about half of the WIM in ordinary star-forming galaxies like M33 (Hoopes & Walterbos 2000) and the Small Magellanic Cloud (Oey et al. 2004). Observations suggest that ionizing radiation escaping from ordinary H II regions can account for the other half of WIM ionization (Oey & Kennicutt 1997; Voges et al. 2005). However, in galaxies with high absolute star-formation rates, the fraction of field OB stars is expected to decrease as (Oey et al. 2004),

$$f_{\mathrm{field}} = \left(\ln N_{*,\mathrm{up}} + 0.5772 \right)^{-1} \quad , \qquad (3)$$

where $N_{*,\mathrm{up}}$ is the number of OB stars in the richest cluster of that galaxy. This assumes a simple power-law relation for the clustering law of the form,

$$N(N_*) \, dN_* \propto N_*^{-2} \, dN_* \quad , \qquad (4)$$

where N_* is the number of OB stars per cluster. This clustering law appears to be universal (e.g., Elmegreen & Efremov 1997) and is supported by observations of super star clusters (Meurer et al. 1995; Zhang et al. 2001) and ordinary H II regions (Oey & Clarke 1998). It also appears to extend down to the individual massive stars in the field (Oey et al. 2004). Therefore, we do expect the contribution of ionization from field stars to decrease from about one-quarter of the total ionizing emission in ordinary star-forming galaxies to about one-tenth in galaxies with the
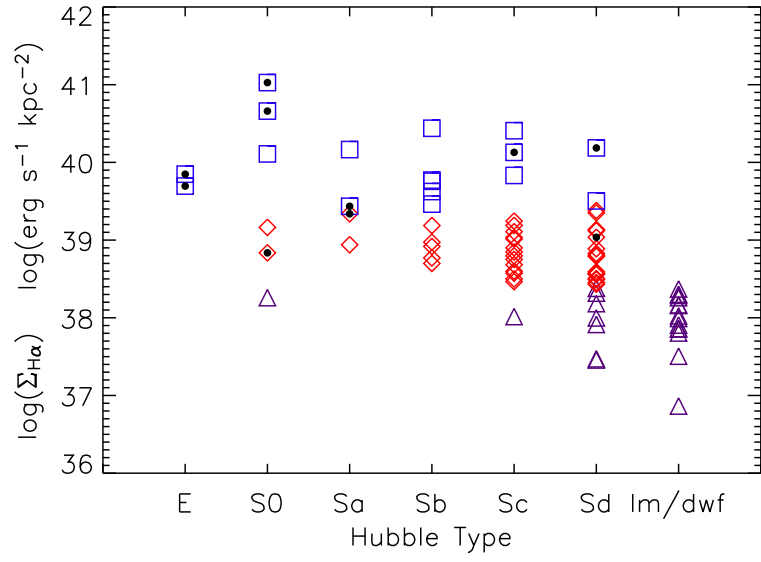
Fig. 9.— Hα surface brightness, a measure of star formation intensity, for different galaxy Hubble types. Symbols are as in Figure 3.
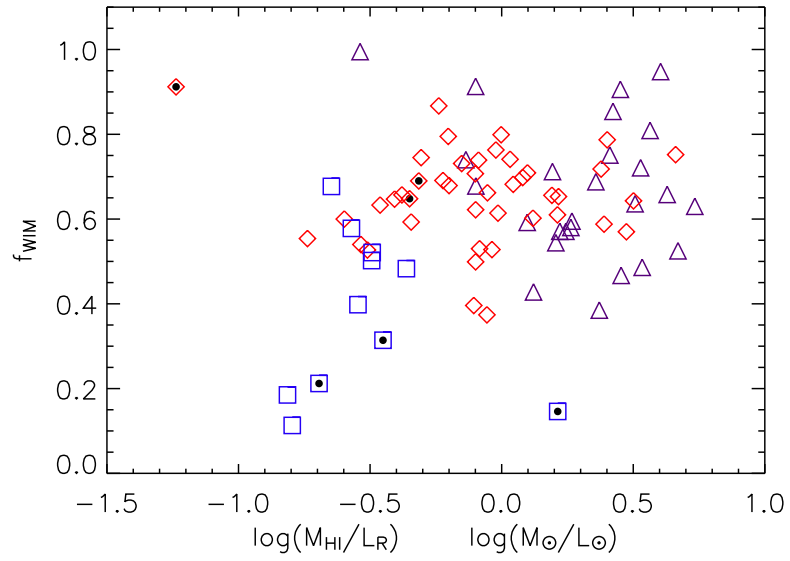

Fig. 10.— Hα diffuse fraction vs galaxy H I gas fraction as measured by $M_{\rm HI}/L_R$. Symbols for different star-formation categories are as in Figure 3, and galaxies which have only upper limits on $M_{\rm HI}$ are omitted for clarity.
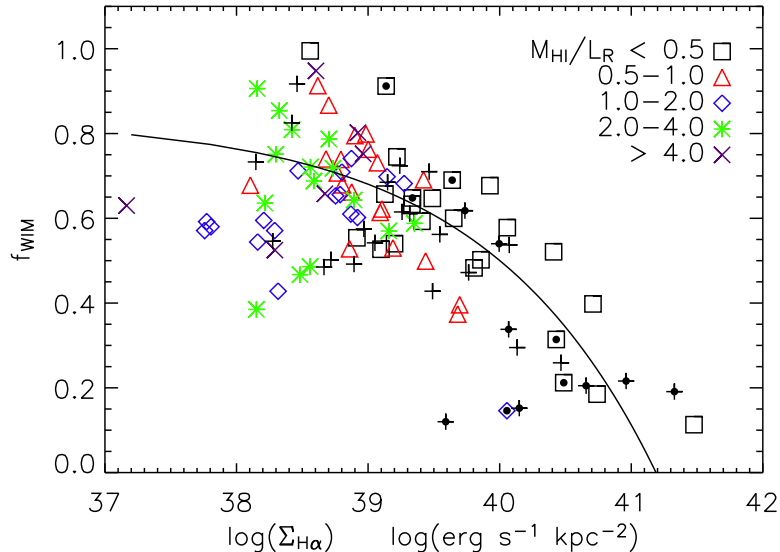
FIG. 11.— Hα diffuse fraction vs Hα surface brightness, a measure of star formation intensity. Symbols correspond to the H I gas fraction M_{HI}/L_R as shown, in units of $M_\odot/L_\odot$, and plus symbols indicate galaxies whose H I gas fractions are only upper limits. Note that starburst galaxies are defined as those having $\log \Sigma_{H\alpha}/(\mathrm{erg\ s^{-1}\ kpc^{-2}}) > 39.4$. The curve has a form given by equation 7.

highest SFR. Since our starburst galaxies, defined as those with the highest SFI, may well have extreme SFRs, a lower fraction of field massive stars is plausible.

We test this possibility in Figure 12, which shows the Hα diffuse fraction vs total Hα luminosity of the sample galaxies. The symbols correspond to the star formation categories as before. Certainly there is no well-defined anti-correlation, as would be expected if this scenario were the origin of that seen in Figure 11. Thus, possibility (1b) above, that starbursts have lower f_{WIM} strictly because of a reduced population of ionizing field OB stars, appears to be ruled out.

We now consider possibility (2a) above, that ionizing radiation escapes from the starbursts, under-ionizing the diffuse ISM. Clarke & Oey (2002) calculated a crude parameterization for a threshold in star formation rate above which galaxies are expected to release ionizing photons and galactic superwinds:

$$\mathrm{SFR_{crit}} = 0.15 \left(\frac{M_{\mathrm{ISM},10}\, \tilde{v}_{10}^2}{f_d} \right)\ M_\odot\ \mathrm{yr^{-1}}\quad , \qquad (5)$$

where $M_{\mathrm{ISM},10}$ is the ISM mass in units of $10^{10}\ M_\odot$, $\tilde{v}_{10}$ is the thermal velocity of the ISM in units of $10\ \mathrm{km\,s^{-1}}$, and f_d is a geometric correction factor for disk galaxies. This relation results from a simple criterion that balances the supernova mechanical energy resulting from star formation against the total ISM thermal energy. If the former dominates, the ISM is shredded, a galactic outflow is generated, and ionizing photons escape. For our SR1 sample, we adopt M_{HI} for the ISM mass. The ISM thermal velocity is roughly the sound speed, which we take to be $10\ \mathrm{km\,s^{-1}}$ for the entire sample. Similarly, we adopt $f_d = 0.1$ for the entire sample, an approximate estimate for disk galaxies. This value for f_d may be an underestimate for earlier types and irregular galaxies, but given the uncertainty and crudeness of the relation in equation 5, we

do not adjust f_d for different galaxy types. Thus, we take $\mathrm{SFR_{crit}}$ to be simply proportional to M_{HI}.

The Hα luminosity is a measure of the total SFR, bearing in mind that if ionizing photons are lost, then $L_{H\alpha}$ is an underestimate of the SFR. We use the same relation as before (equation 2) to estimate values for $L_{H\alpha,\mathrm{crit}}$ from the computed $\mathrm{SFR_{crit}}$. In Figure 13, we show $L_{H\alpha}/L_{H\alpha,\mathrm{crit}}$ vs SFI. Roughly half the sample shows $L_{H\alpha}/L_{H\alpha,\mathrm{crit}} > 1$, suggesting that our crude relation estimating $\mathrm{SFR_{crit}}$ (equation 5) may be subject to a scaling effect with a factor of a few, but is not unreasonable. Inclusion of molecular ISM, for example, can be critical (e.g., Young & Knezek 1989; Keres et al. 2003) and would reduce the number of galaxies exceeding this criterion. The symbols in Figure 13 are plotted according to M_{HI}/L_R, showing that the galaxies with the lowest H I gas fractions have the highest $L_{H\alpha}/L_{H\alpha,\mathrm{crit}}$. There is also a hint of flattening in the correlation between $L_{H\alpha}/L_{H\alpha,\mathrm{crit}}$ and SFI, which may simply be a bias that underestimates the extinctions for starburst galaxies (see Paper I). But if it is real, it may suggest that $L_{H\alpha}$ underestimates the star formation and ionizing radiation for the most extreme objects. Such a trend, along with the lower H I gas fraction for the starbursts is consistent with the escape of Lyman continuum radiation from such galaxies. However, regardless of any flattening, Figure 13 crudely confirms the plausibility that the starburst galaxies have $\mathrm{SFR} > \mathrm{SFR_{crit}}$ for the escape of ionizing radiation.

Figure 14 shows $L_{H\alpha}/L_{H\alpha,\mathrm{crit}}$ vs f_{WIM}, plotted by SFI category. The starburst galaxies, which have low f_{WIM}, have relatively higher $L_{H\alpha}/L_{H\alpha,\mathrm{crit}}$ compared to the remainder of the sample. We note that although previous studies reported that starburst galaxies are optically thick to ionizing photons (e.g., Heckman et al. 2001; Leitherer et al. 1995), Shapley et al. (2006) recently reported unambiguous detection of Lyman continuum radiation from individual galaxies at $z \sim 3$, and Bergvall et al. (2006) also

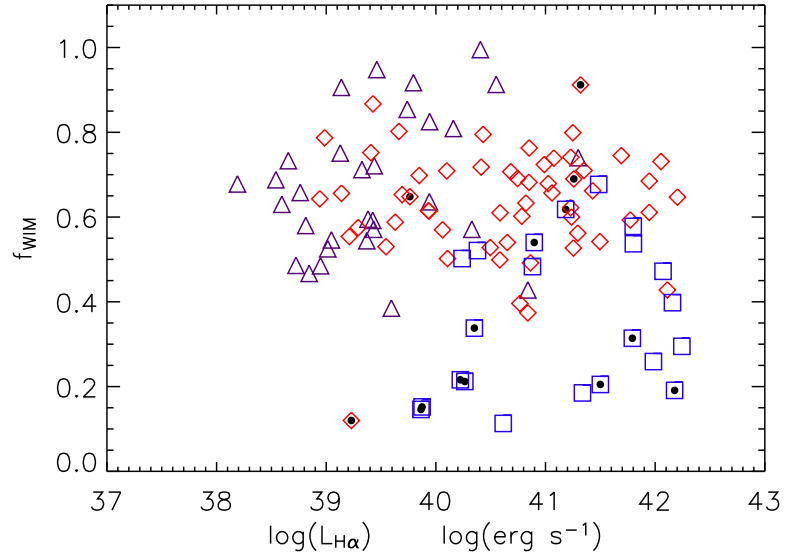Fig. 12.— f_{WIM} vs total star formation rate as measured by galaxy total Hα luminosity. Symbols for different star-formation categories are as in Figure 3.

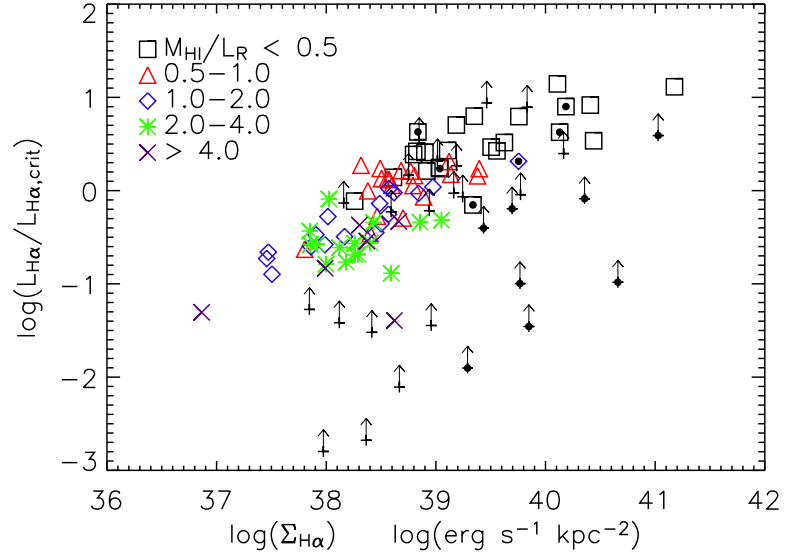Fig. 13.— $L_{\mathrm{H}\alpha}/L_{\mathrm{H}\alpha,\mathrm{crit}}$ vs Hα surface brightness, a measure of star formation intensity. Symbols show the H$_{\mathrm{I}}$ gas fraction as in Figure 11, and arrows indicate lower limits.
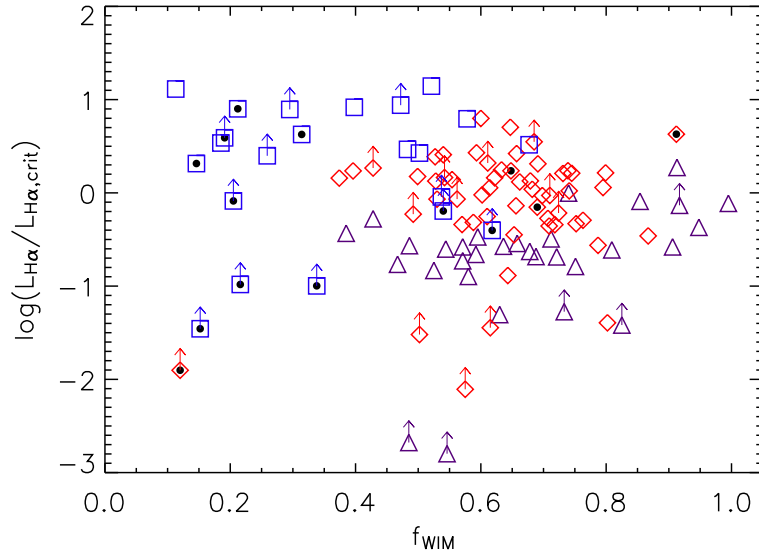
Fig. 14.— $L_{H\alpha}/L_{H\alpha,crit}$ vs Hα diffuse fraction. Symbols are as in Figure 3.

detect Lyman continuum emission from the blue compact dwarf Haro 11. In addition, radiative feedback from the Milky Way appears to be responsible for ionizing nearby high velocity clouds (e.g., Bland-Hawthorn & Maloney 1999; Putman et al. 2003), which seems to be consistent with the prediction from equation 5 (Clarke & Oey 2002). However, all of the positive detections imply escape fractions of $\lesssim 0.1$.

Figures 13 and 14 show that the low fractions of diffuse Hα emission in starburst galaxies are qualitatively fully consistent with a predicted threshold SFR for escaping ionizing radiation. Indeed, these survey data suggest that the crude prediction given by equation 5 is not only meaningful, but also that we may be able to calibrate it with a somewhat larger dataset, for example, the full SINGG sample. Note that while equation 5 predicts the loss of ionizing photons from galaxies, it is not based on an actual density-bounding criterion caused directly by photoionization. Thus it can straightforwardly account for the co-existence of some neutral gas *and* substantial losses of ionizing radiation. This is fully consistent with the observations for our sample. SFR$_{crit}$ is instead based on an over-pressure criterion, in which star formation drives the ISM pressure. The higher temperatures determined for the WIM in the starburst galaxy M82 by Shopbell & Bland-Hawthorn (1998) imply higher thermal pressures, supporting this scenario. Our over-pressure criterion is essentially the same model considered by Wang, Heckman, & Lehnert (1998) to explain the anticorrelation of [S II]/Hα with SFI for actively star-forming galaxies. They separately considered ISM pressure regulated by mechanical feedback and by simple hydrostatic equilibrium. The Clarke & Oey (2002) relation (equation 5) considers both of these as components of a unified system, so our SINGG results also point to pressure regulation of WIM and other feedback properties, like outflows and superwinds, that are directly driven by star formation.

Finally, we note possibility (2b) above, that the huge

H II regions in starbursts have the appearance of almost fully occupying the ISM of their host galaxies, suggestive that the diffuse WIM is the small, remaining fraction in a density-bounded situation. For ionization-bounded conditions, a galaxy's total Strömgren volume scales directly with the sum of all the H II region luminosities, assuming the escape fraction of photons from H II regions into the WIM remains constant. Therefore, f_{WIM} also remains constant, with the WIM again defined as the Hα emission exterior to the H II regions. However, for density-bounded situations, a maximum possible Strömgren volume is reached, and thus the WIM shrinks as the H II regions grow. If this is the cause of our observed decrease in f_{WIM}, then it should roughly follow a relation,

$$f_{WIM} \sim V_{S,gal} - \sum R_{HII}{}^3 \quad, \qquad (6)$$

where $V_{S,gal}$ is the maximum possible Strömgren volume, and R_{HII} are the individual H II region radii. The total volume in H II regions scales directly with the SFR, while $V_{S,gal}$ is constant, so:

$$f_{WIM} \sim V_{S,gal} - L_{H\alpha}^{1/3} \quad, \qquad (7)$$

ignoring coefficients. The curve overplotted in Figure 11 shows this $-L_{H\alpha}^{1/3}$ relation, scaled arbitrarily. This ignores the different galaxy sizes, which would introduce a dispersion in the relation. The curve shows a remarkable agreement with the data, and thus, density-bounding in the inner volumes of galaxies is another possibility to explain the lower f_{WIM} in starbursts. This would require the observed H I to be in the outer disks of such galaxies. Putman et al. (2003) discuss these geometric considerations concerning the escape of ionizing radiation from the Milky Way.

If the loss of ionizing radiation is indeed the origin of the low Hα diffuse fraction in our starburst galaxies, then the implied fractions of total Lyman continuum emission escaping into the IGM are uncomfortably large, especially

in view of the fact that we have no truly extreme examples of starbursts in our sample. If $f_{\rm WIM}$ is reduced by a factor of two or more, as seen in many objects, then the implied escape fraction of ionizing radiation is on the order of 25%. This is much larger than fractions of $\lesssim 5\%$ that have been measured by direct, but very few, Lyman continuum observations. It is therefore likely that more than one process is responsible for the observed reduced $f_{\rm WIM}$ in galaxies with the highest SFI. For example, possibility (1a) above remains: that high dust content in starbursts is absorbing a disproportionate fraction of the Lyman continuum emission. It may also be, as suggested by Dopita et al. (2006), that the WIM is composed largely of highly evolved, filamentary H II regions, and that these are fractionally underrepresented in starbursts. Further study is necessary to clarify all of the possible models. We note that if ionizing radiation is indeed escaping from these galaxies, then models suggesting that the bulk of H I in galaxies is due to photodissociation of large reservoirs of molecular gas (e.g., Allen 2001) are not supported by this result, since we see a decrease in both $f_{\rm WIM}$ and the H I gas fraction in starbursts.

5. CONCLUSION

We have used the SINGG SR1 dataset to study the properties of the diffuse, warm ionized medium across the range of galaxy properties represented in this H I-selected sample. The mean fraction of diffuse Hα emission from our galaxies is 0.59 ± 0.19, somewhat higher than found in previous studies. We attribute much of this difference to the lack of optical bias in our sample. As with other studies, we find no correlations in $f_{\rm WIM}$ with Hubble type.

However, starburst galaxies, defined here as those having Hα surface brightness $> 2.5 \times 10^{39}$ erg s^{-1} kpc^{-2}, show substantially lower $f_{\rm WIM}$ compared to other galaxies. We caution that the magnitude of this result is sensitive to the method of determining $f_{\rm WIM}$, but the Hα surface brightness distributions show it to be real. We note that [S II]/Hα and [N II]/Hα ratios, which are high in the WIM, are similar between normal galaxies and starbursts (e.g., Lehnert & Heckman 1994; Kewley et al. 2001), consistent with $f_{\rm WIM}$ in starbursts being no larger than that in normal star-forming galaxies. The effect of a lower $f_{\rm WIM}$ in starbursts does not appear to be dominated by a lower fraction of field OB stars. However, it is broadly consistent with the prediction that ionizing radiation is escaping from galaxies having total star-formation rates above a critical threshold predicted by Clarke & Oey (2002). This prediction derives from an ISM over-pressure criterion, based on star formation driving the ISM pressure and resulting WIM properties. Wang et al. (1998) also suggested that the WIM ionization state is determined by such a mechanism. Supporting this interpretation, we also find that galaxies with the highest star-formation intensities tend to be those with the lowest H I gas fractions, suggesting that the gas has been consumed and/or ionized by star-formation. The data are also consistent with pure density-bounding of the central regions in these galaxies. If either of these models is correct, then it implies that ionizing radiation is escaping from most starburst galaxies, with an inferred escape fraction that may be as large as 25% for this sample. However, in view of the contradictory results in the literature that suggest much lower escape fractions, it is likely that other processes contribute to the reduction of the observed $f_{\rm WIM}$.

REFERENCES

Allen, R. J. 2001, in *Gas and Galaxy Evolution,* J. Hibbard, M. Rupen, & J. van Gorkom (eds.), ASP Conf. Ser. 240, (San Francisco: ASP), 331

Banfi, M., Rampazzo, R., Chincarini, G., & Henry, R. B. C., 1993, A&A, 280, 373

Barnes, D. G., et al. , 2001, MNRAS, 322, 486

Bergvall, N., Zackrisson, E., Andersson, B.-G., Arnberg, D., Masegosa, J., & Östlin, G. 2006, A&A 448, 513

Bland-Hawthorn, J. & Maloney, P. R. 1999, ApJ 510, L33

Bland-Hawthorn, J. & Putman, M. 2001, in *Gas and Galaxy Evolution,* J. Hibbard, M. Rupen, & J. van Gorkom (eds.), ASP Conf. Ser. 240, (San Francisco: ASP), 369

Clarke, C. J. & Oey, M. S. 2002, MNRAS, 337, 1299

Collins, J. A. & Rand, R. J., 2001, ApJ, 551, 57

Deharveng, L., Caplan, J. Lequeux, J., Azzopardi, M., Breysacher, J., Tarenghi, M., & Westerlund, B. 1988, A&AS 73, 407

Dopita, M. A., et al., 2006, ApJ, 647, 244

Elmegreen, B. G. & Efremov, Y. N., 1997, ApJ, 480, 235

Ferguson, A. M. N., Wyse, R. F. G., Gallagher, J. S., & Hunter, D. A., 1996, AJ, 111, 2265

Hanish, D. J., et al. 2006, ApJ, 649, 150

Heckman, T. M., Sembach, K. R., Meurer, G. R., Leitherer, C., Calzetti, D., & Martin, C. L. 2001, ApJ 558, 56

Heckman, T. M. 2005, in *Starbursts: From 30 Doradus to Lyman Break Galaxies,* R. de Grijs & R. M. González Delgado (eds.), Ap&SS Library, 329, 3

Helmboldt, J. F., Walterbos, R. A. M., Bothun, G. D., & O'Neil, K., 2005, ApJ 630, 824

Hoopes, C. G. & Walterbos, R. A. M. 2000, ApJ 541, 597

Hoopes, C. G., Walterbos, R. A. M., & Greenawalt, B. E., 1996, AJ, 112, 1429

Karachentsev, I. D., Karachentseva, V. E., Huchtmeier, W. K., & Markov, D. I. 2004, AJ, 127, 2031

Kennicutt, R. C. 1998, ARAA, 36, 189

Kennicutt, R. C., Edgar, B. K., & Hodge, P. W., 1989, ApJ, 337, 761

Kennicutt, R. C., Tamblyn, P., & Congdon, C. E. 1994, ApJ, 435, 22

Keres, D., Yun, M. S., & Young, J. S. 2003, ApJ, 582, 659

Kewley, L. J., Dopita, M. A., Sutherland, R. S., Heisler, C. A., & Trevena, J. 2001, ApJ 556, 121

Knapen, J. H., 1998, MNRAS, 297, 255

Koribalski, B. S., et al. 2004, AJ 128, 16

Leitherer, C., Ferguson, H. C., Heckman, T. M., & Lowenthal, J. 1995, ApJ 454, L19

Lehnert, M. D. & Heckman, T. M. 1994, ApJ 426, L27

Maddox, S. J., Sutherland, W. J., Efstathiou, G., & Loveday, J. 1990, MNRAS, 243, 692

McCall, M. L., Straker, R. W., & Uomoto, A. K., 1996, AJ, 112, 1096

Meurer, G. R., et al. 2006, ApJS, 165, 307

Meurer, G. R., Heckman, T. M., Leitherer, C., Kinney, A., Robert, C., & Garnett, D. R., 1995, AJ, 110, 2665

Meurer, G. R., Heckman, T. M., Lehnert, M. D., Leitherer, C., & Lowenthal, J. 1997, AJ 114, 54

Meyer, M. J., et al. 2004, MNRAS 350, 1195

Mould, J. R., et al. 2000, ApJ 529, 786

Oey, M. S. & Kennicutt, R. C. 1997, MNRAS 291, 827

Oey, M. S., King, N. L., & Parker, J. W. 2004, AJ, 127, 1632

Oey, M. S. & Clarke, C. J. 1998, AJ, 115, 1543

O'Neil, K., Oey, M. S., & Bothun, G. 2007, ApJ, submitted

Putman, M. E., Bland-Hawthorn, J., Veilleux, S., Gibson, B. K., Freeman, K. C., & Maloney, P. R. 2003, ApJ 597, 948

Rand, R. J., 1992, 103, 815
Reynolds R. J. 1984, ApJ, 282, 191
Reynolds, R. J., Haffner, L. M., & Tufte, S. L., 1999, ApJ, 525, L21
Rossa, J. & Dettmar, R.-J. 2003, A&A 406, 505
Shapley, A. E., Steidel, C. C., Pettini, M., Adelberger, K. L., & Erb,
    D. K. 2006, ApJ 651, 688
Shopbell, P. L. & Bland-Hawthorn, J. 1998, ApJ 493, 129
Thilker, D. A., Braun, R., & Walterbos, R. A. M., 2000, AJ, 120,
    3070
Thilker, D. A., Walterbos, R. A. M., Braun, R., & Hoopes, C. G.
    2002, AJ, 124, 3118

Veilleux, S., Cecil, G., & Bland-Hawthorn, J. 1995, ApJ 445, 152
Voges, E. S., Walterbos, R. A. M., Hoopes, C. G., & Oey, M. S. 2005,
    in *Extra-Planar Gas*, R. Braun, ed., ASP Conf. Series 331, 225
Wang, J., Heckman, T. M., & Lehnert, M. D. 1998, ApJ 509, 93
Wang, J., Heckman, T. M., & Lehnert, M. D. 1999, ApJ 515, 97
Walterbos, R. A. M., 1998, PASA, 15, 99
Young, J. S. & Knezek, P. M. 1989, ApJ, 347, L55
Zhang, Q., Fall, S. M., & Whitmore, B. C. 2001, ApJ 561, 727
Zurita, A., Rozas, M., & Beckman, J. E. 2000, A&A 363, 9
Zurita, A., Beckman, J. E., Rozas, M., & Ryder, S. 2002, A&A 386,
    801

TABLE 1
SINGG SR1 GALAXY PARAMETERS

HIPASS ID	Optical ID	Hubble type	Dist (Mpc)	i (deg)	TG[a]	$\log M_{HI}$ (log $M_\odot$)	$\log L_R$ (log $L_\odot$)	$\log L_{H\alpha}$ (log erg s^{-1})	$\log \Sigma_{H\alpha}$ (log erg s^{-1} kpc^{-2})	f_{WIM}	$\log \mathrm{SFR}_{crit}$ (log $M_\odot$ yr^{-1})
J0005-28	ESO409-IG015	Double?system*	10.6	56.6	1.75	8.27	8.06	39.86	39.75	0.15	−1.55
J0019-22	MCG-04-02-003	Im:pec	9.8	53.0	3.50	8.55	8.05	38.94	38.59	0.64	−1.27
J0031-22	ESO473-G024	IB(s)m	7.9	57.5	4.00	8.01	7.48	38.72	38.26	0.49	−1.81
J0039-14a	NGC178	SB(s)m	20.6	64.7	1.00	9.40	9.46	40.84	39.38	0.37	−0.42
J0043-22	IC1574	IB(s)m	5.5	56.8	2.00	7.54	7.64	38.19	37.80	0.68	−2.28
J0135-41	NGC625	SB(s)m?sp_HII	5.1	74.8	3.00	8.09	8.78	40.26	40.19	0.21	−1.74
J0145-43	ESO245-G005	IB(s)m	4.4	55.3	4.50	8.58	8.31	39.38	37.91	0.60	−1.25
J0156-68	ESO052-G010	Dwarf	19.0	61.9	1.25	8.54	8.35	39.33	38.17	0.71	−1.28
J0209-10:S1	NGC839	Spec_sp;LINER_Sy2	54.3	68.8	0.50	<10.31	10.25	41.50	40.36	0.20	<0.49
J0209-10:S2	NGC838	SA(rs)0ô_pec:Sbrst	54.3	44.4	0.50	<10.31	10.32	42.18	41.03	0.19	<0.49
J0209-10:S3	NGC835	SAB(r)ab:_pec._LINER	54.3	65.8	0.75	<10.31	10.61	41.98	40.17	0.26	<0.49
J0209-10:S4	NGC833	(R')Sa:pec;Sy2_LINER	54.3	67.2	0.75	<10.31	10.34	41.18	39.44	0.62	<0.49
J0216-11c	NGC873	Sc	55.9	43.8	0.75	9.96	10.51	42.16	40.41	0.40	0.14
J0221-05:S1	NGC895	SA(s)cd	31.9	47.0	1.75	<10.06	10.26	41.50	38.75	0.54	<0.23
J0221-05:S2	NGC895A	E	31.9	34.7	1.25	<10.06	8.23	39.87	39.85	0.15	<0.23
J0223-04	APM[b]	...	31.6	53.0	1.25	9.49	8.93	40.16	38.12	0.81	−0.33
J0224-24:S1	NGC922	SB(s)cd_pec	43.1	23.7	0.75	<10.07	10.35	42.24	39.83	0.29	<0.25
J0224-24:S2	2MASX[c]	...	43.1	40.1	1.00	<10.07	9.08	40.35	39.77	0.34	<0.25
J0240-08	NGC1042	SAB(rs)cd	19.2	29.7	1.50	9.59	10.10	41.25	38.80	0.53	−0.23
J0256-54	ESO154-G023	SB(s)m	7.1	90.0	2.50	9.24	8.73	39.94	37.91	0.64	−0.59
J0309-41	ESO300-G014	SAB:(s)dm	12.9	63.7	3.50	9.00	9.10	40.55	38.32	0.91	−0.82
J0310-39	ESO300-G016	IAB(s)m:pec	9.4	51.1	4.00	7.95	7.59	38.54	38.29	0.69	−1.88
J0314-04	DDO032	IB(s)m	31.0	44.7	2.00	9.53	9.41	40.78	38.62	0.60	−0.29
J0317-22	ESO481-G017	SAB(r)ab	55.0	22.2	0.50	10.14	10.45	41.26	39.34	0.69	0.31
J0317-41	NGC1291	(R_1)SB(l)0/a	11.2	32.0	2.75	9.41	10.65	41.32	38.84	0.91	−0.41
J0320-52	NGC1311	SB(s)m	7.0	71.2	2.50	8.25	8.60	39.76	39.04	0.65	−1.57
J0322-04	NGC1314	SA(rs)d	55.0	41.1	0.50	10.02	10.16	41.30	38.38	0.74	0.20
J0333-50	IC1959	SB(s)m:sp	8.1	80.5	3.00	8.61	8.62	39.94	38.79	0.61	−1.22
J0341-01	APM[b]	...	47.9	5.0	0.50	9.63	9.41	40.33	37.99	0.57	−0.19
J0342-13:S1	NGC1421	SAB(rs)bc:	29.1	77.4	1.00	<9.85	10.39	42.07	39.46	0.47	<0.03
J0342-13:S2	APM[b]	...	29.1	57.6	0.75	<9.85	7.85	39.23	39.29	0.12	<0.03
J0345-35	ESO358-G060	IB(s)m:sp	10.8	73.6	3.50	8.46	7.80	39.41	38.66	0.75	−1.36
J0348-39	ESO302-G?010	IB(s)m	16.0	43.1	0.50	8.43	8.17	38.81	37.51	0.58	−1.39
J0349-48	IC2000	SB(s)cd:sp	13.1	74.8	2.50	9.10	9.30	40.43	38.60	0.80	−0.73
J0351-38	ESO302-G014	Im_pec	11.7	47.3	2.00	8.55	8.13	39.74	38.02	0.85	−1.27
J0355-42	NGC1487	Pec*	11.2	70.2	3.00	9.25	9.36	40.77	39.40	0.40	−0.57
J0359-45:S1	Hor_Dwarf	IB(s)m	11.9	55.9	2.50	<8.65	8.14	39.79	38.16	0.92	<−1.17
J0359-45:S2	ESO249-G035	SBcd:sp	11.9	65.4	1.75	<8.65	7.70	38.65	37.85	0.73	<−1.17
J0403-43:S1	NGC1512	SB(r)ab	12.0	15.4	4.50	<9.93	9.99	40.99	38.94	0.72	0.11
J0403-43:S2	NGC1510	SA00^_pec?;HIIBCDG	12.0	28.5	1.75	<9.93	8.93	40.22	40.66	0.22	<0.11
J0404-02	NGC1507	SB(s)m-pec?	12.4	76.7	3.00	9.16	9.38	40.74	39.12	0.69	−0.67
J0409-56	NGC1533	(L)SB(rs)0ô	10.1	28.1	2.50	9.24	9.78	40.41	38.26	1.00	−0.58
J0412+02	UGC2983	SB(s)b:	70.5	74.7	0.75	10.20	10.51	41.69	38.92	0.75	0.38
J0430-01	UGC3070	SAB(s)b_pec:	36.1	49.2	1.00	9.53	9.49	40.85	38.97	0.68	−0.29
J0433-75	IC2089	SAB(r)dm	69.0	41.2	1.00	9.79	9.89	41.23	38.80	0.62	−0.03
J0441-02	NGC1637	SAB(rs)c	10.4	38.0	2.75	9.30	9.76	40.82	39.03	0.63	−0.53
J0454-53	NGC1705	SA0-_pec:;HIIBCDG	7.6	45.1	3.00	7.96	8.45	40.38	40.11	0.52	−1.87
J0457-42	ESO252-IG001	Double_system*	8.3	51.0	4.50	8.27	7.87	38.99	38.40	0.79	−1.55
J0459-26	NGC1744	SB(s)d	10.0	55.5	5.50	9.56	9.35	40.58	38.57	0.61	−0.26
J0503-25	ESO486-G021	S?	11.4	54.2	4.50	8.60	8.52	39.85	38.84	0.70	−1.22
J0503-63:S1	ESO085-G034	S0	70.4	37.6	0.50	<10.10	10.57	41.35	39.16	0.71	<0.28
J0503-63:S2	ESO085-G034	...	70.4	26.4	0.75	<10.10	8.77	39.93	38.96	0.62	<0.28
J0504-16:S1	MCG-03-13-063	SB?	47.7	55.4	1.00	<10.08	9.71	41.29	39.24	0.56	−0.26
J0504-16:S2	...	...	47.7	33.8	0.50	<10.08	8.41	39.94	38.12	0.82	−0.26
J0506-31	NGC1800	IB(s)m_HII	10.9	50.7	2.25	8.54	9.03	40.24	39.56	0.50	−1.29
J0507-16	DDO036	SB(s)m	29.1	40.9	1.50	9.56	9.65	41.08	38.49	0.74	−0.26
J0507-37	NGC1808	(R'_1)SAB(s):b_Sy2	13.5	64.4	2.00	9.53	10.34	41.34	40.44	0.19	−0.30
J0510-31	UGCA103	SB(r)dm	13.3	49.2	1.75	9.09	9.13	40.50	38.56	0.53	−0.73
J0512-32	UGCA106	SAB(s)m	12.6	45.9	5.00	9.48	9.10	40.41	38.43	0.72	−0.35

TABLE 1

— CONTINUED

HIPASS ID	Optical ID	Hubble type	Dist (Mpc)	i (deg)	TG[a]	$\log M_{\rm HI}$ (log $M_\odot$)	$\log L_R$ (log $L_\odot$)	$\log L_{\rm H\alpha}$ (log erg s^{-1})	$\log \Sigma_{\rm H\alpha}$ (log erg s^{-1} kpc^{-2})	$f_{\rm WIM}$	SFR$_{\rm crit}$ (log erg s^{-1})
J0943−05b	UGCA175	SB(s)dm	31.8	40.5	1.50	9.36	9.74	41.06	38.83	0.66	−0.46
J0943−09b	MCG-02-25-013	SAB(s)d	41.6	71.8	1.25	9.93	9.90	41.23	38.57	0.74	0.11
J1002−06	UGCA193	Sdm	7.4	80.1	4.50	8.64	8.23	39.13	38.00	0.75	−1.18
J1018−17	NGC3200	SA(rs)bc	53.2	76.8	1.00	10.57	10.72	42.05	38.77	0.73	0.74
J1046+01	NGC3365	Scd	12.2	77.3	4.00	9.18	9.08	40.10	38.50	0.71	−0.65
J1051−19	ESO569-G014	SB(s)cd:	31.0	90.0	1.50	9.76	9.76	41.25	38.68	0.80	−0.07
J1054−18:S1	ESO569-G020	SA(rs)d:	62.4	42.9	0.75	< 9.81	9.62	40.86	38.59	0.49	< −0.01
J1054−18:S2	ESO569-G021	E?	62.4	38.5	0.75	< 9.81	9.55	40.90	39.69	0.54	< −0.01
J1105−00	NGC3521	SAB(rs)bc_LINER	8.6	59.1	6.50	9.69	10.34	41.49	39.62	0.68	−0.13
J1106−14	KKS2000-23	Ir	12.7	64.6	2.00	8.62	7.89	38.60	36.86	0.63	−1.20
J1109−23	IC2627	SAB(rs?)bc	31.0	36.1	1.75	9.73	10.30	41.80	39.76	0.58	−1.09
J1123−08	NGC3660	SB(r)bc_Sy2	56.5	44.6	1.25	10.22	10.63	42.20	39.19	0.65	0.40
J1131−02:S1	UGC6510	SAB(rs)cd	72.9	14.8	1.00	<10.35	10.54	41.95	39.01	0.61	< 0.53
J1131−02:S2	APM[b]	...	72.9	41.7	0.75	<10.35	9.14	40.11	38.42	0.50	< 0.53
J1131−02:S3	...	...	72.9	46.3	0.50	<10.35	7.03	38.95	38.36	0.49	< 0.53
J1217+00	UGC7332	IB(s)m	8.9	53.8	6.00	8.57	7.90	39.01	37.99	0.52	−1.25
J1231−08	NGC4487	SAB(rs)cd	11.1	50.9	4.00	8.97	9.50	40.65	38.90	0.54	−0.86
J1235−07	UGCA289	SAB(s)dm	10.4	62.7	4.50	8.81	8.71	39.42	37.47	0.59	−1.02
J1253−12	UGCA307	IB(s)m	8.6	65.0	5.00	8.67	8.28	39.63	39.05	0.59	−1.15
J1303−17c	UGCA320	IB(s)m_sp	7.7	78.2	4.00	9.12	8.65	40.06	38.86	0.57	−0.70
J1318−21	NGC5068	SB(s)d	6.9	26.3	5.00	9.16	9.76	41.24	39.35	0.60	−0.66
J1337−28	ESO444-G084	Im	5.9	42.6	6.00	8.03	7.40	38.76	38.37	0.66	−1.79
J1337−29	NGC5236	SAB(s)c;HIISbrst	4.9	11.3	6.00	9.89	10.34	41.79	40.13	0.31	0.07
J1339−31A	NGC5253	Im_pec;HII_Sbrst	3.3	62.8	7.50	10.87	9.02	40.61	41.18	0.11	−1.60
J1341−29	NGC5264	IB(s)m	4.4	37.6	9.00	7.79	8.53	39.21	38.61	0.55	−2.03
J1954−58	IC4901	SAB(r)c	31.1	35.6	1.00	10.07	10.41	41.77	39.11	0.59	0.24
J2009−61	IC4951	SB(s)dm:sp	11.2	76.7	3.00	8.87	8.65	39.69	38.45	0.65	−0.96
J2052−69	IC5052	SBd:sp	7.5	90.0	2.75	9.13	9.23	40.58	39.14	0.50	−0.69
J2102−16	IC5078	SA(s)cd:	23.0	68.9	1.75	9.68	9.78	40.68	38.47	0.71	−0.14
J2149−60:S1	NGC7125	SAB(s)c	45.5	40.9	0.75	<10.57	10.41	42.11	39.19	0.43	< 0.74
J2149−60:S2	NGC7126	SA:(rs:)bc	45.5	56.7	0.75	<10.57	10.43	41.80	39.77	0.54	< 0.74
J2149−60:S3	ESO145-G018A	...	45.5	45.4	0.75	<10.57	8.09	39.05	37.97	0.55	< 0.74
J2202−20:S1	NGC7184	SB(r)c	38.6	73.8	0.75	<10.12	10.78	41.95	38.85	0.69	0.30
J2202−20:S2	APM[b]	...	38.6	56.3	0.75	<10.12	8.18	39.29	38.67	0.57	< 0.30
J2214−66	IC5176	SAB(s)bc?_sp	24.8	83.0	1.25	9.87	9.89	40.85	38.70	0.76	0.04
J2217−42	APM[b]	...	31.9	51.7	1.00	8.85	8.32	39.44	38.26	0.72	−0.98
J2220−46	IC5201	SB(s)cd	13.2	67.1	1.50	9.84	9.72	40.84	38.01	0.43	0.02
J2222−48	ESO238-G005	IABm	10.1	47.2	1.75	8.55	7.95	39.46	38.30	0.95	−1.27
J2234−04	MCG-01-57-015	IBm	14.1	63.3	1.75	8.70	8.49	39.37	37.86	0.54	−1.13
J2257−41	NGC7424	SAB(rs)cd	13.6	39.0	1.75	10.04	10.09	41.43	38.57	0.66	0.21
J2257−42	NGC7412A	SBdm:sp	13.4	78.1	2.00	8.88	8.64	39.43	37.46	0.57	−0.94
J2326−37	ESO347-G017	SB(s)m:sp	10.0	68.5	1.75	8.34	8.42	39.54	38.89	0.53	−1.49
J2334−36	IC5332	SA(s)d	10.1	30.8	2.75	9.62	9.82	41.03	38.50	0.68	−0.20
J2334−45b	ESO291-G031	SB_pec	21.2	52.4	1.00	8.75	8.38	39.59	37.85	0.38	−1.07
J2336−37a	NGC7713	SB(r)d:	9.9	64.4	2.50	9.14	9.50	40.88	39.50	0.48	−0.69
J2343−31	UGCA442	SB(s)m:sp	3.8	68.2	4.50	8.33	7.88	38.84	38.18	0.47	−1.49
J2349−37	ESO348-G009	IBm	9.2	64.6	1.50	8.44	7.99	39.14	37.86	0.91	−1.38
J2352−52	ESO149-G003	IB(s)m:sp	7.7	72.7	3.50	8.00	7.81	39.14	38.49	0.66	−1.82

[a] HIIphot terminal gradient, in pc cm^{-6} pc^{-1}.

[b] Galaxy identified in the Automatic Plate Measuring facility survey (Maddox et al. 1990); full APM designation available via NED.

[c] Full designation = 2MASXJ02243002-2444441.

[d] J0403−01 has a lot of Galactic diffuse Hα emission and a bright foreground star, and so its measurements are extremely uncertain.

[e] Hα imaging of J2023−31 was off-center and is likely to be confused with another galaxy in the HI beam.